Published in final edited form as:
Anal Chem. 2007 February 15; 79(4): 1369–1376. doi:10.1021/ac061542n.

A Gravity-Driven Microfluidic Particle Sorting Device with Hydrodynamic Separation Amplification

Dongeun Huh[†], **Joong Hwan Bahng**[†], **Yibo Ling**[†], **Hsien-Hung Wei**[†], **Oliver D. Kripfgans**[‡], **J. Brian Fowlkes**[‡], **James B. Grotberg**[†], and **Shuichi Takayama**[†,§,*]

[†]*Department of Biomedical Engineering, University of Michigan, Ann Arbor, MI 48109-2099*

[‡]*Department of Radiology, University of Michigan, Ann Arbor, MI 48109-0553*

[§]*Department of Macromolecular Science and Engineering, University of Michigan, Ann Arbor, MI 48109-1055*

Abstract

This paper describes a simple microfluidic sorting system that can perform size-profiling and continuous mass-dependent separation of particles through combined use of gravity (1g) and hydrodynamic flows capable of rapidly amplifying sedimentation-based separation between particles. Operation of the device relies on two microfluidic transport processes: i) initial hydrodynamic focusing of particles in a microchannel oriented parallel to gravity, ii) subsequent sample separation where positional difference between particles with different mass generated by sedimentation is further amplified by hydrodynamic flows whose streamlines gradually widen out due to the geometry of a widening microchannel oriented perpendicular to gravity. The microfluidic sorting device was fabricated in poly(dimethylsiloxane) (PDMS), and hydrodynamic flows in microchannels were driven by gravity without using external pumps. We conducted theoretical and experimental studies on fluid dynamic characteristics of laminar flows in widening microchannels and hydrodynamic amplification of particle separation. Direct trajectory monitoring, collection, and post-analysis of separated particles were performed using polystyrene microbeads with different sizes to demonstrate rapid (< 1 min) and high-purity (> 99.9 %) separation. Finally, we demonstrated biomedical applications of our system by isolating small-sized (diameter < 6 μm) perfluorocarbon liquid droplets from polydisperse droplet emulsions, which is crucial in preparing contrast agents for safe, reliable ultrasound medical imaging, tracers for magnetic resonance imaging, or transpulmonary droplets used in ultrasound-based occlusion therapy for cancer treatment. Our method enables straightforward, rapid real-time size-monitoring and continuous separation of particles in simple stand-alone microfabricated devices without the need for bulky and complex external power sources. We believe that this system will provide a useful tool o separate colloids and particles for various analytical and preparative applications, and may hold 3 potential for separation of cells or development of diagnostic tools requiring point-of-care sample preparation or testing.

Introduction

Separation and isolation of particulate materials according to their mass are often crucial steps in sample characterization and preparation for a multitude of applications involving living cells[1,2], macromolecules[3], industrial colloids and particles[4,5], synthetic polymers[6], pharmaceutical emulsions and liposomes[7], and environmental materials[8,9]. The widespread need for mass-dependent separation with high selectivity and resolution has driven the

*To whom correspondence should be addressed: E-mail: takayama@umich.edu.

development of separation techniques such as centrifugation[10], field-flow fractionation (FFF)[11], split-flow thin (SPLITT) fractionation[12], capillary electrophoresis[13,14], elutriation[15], size-exclusion chromatography[16], and hydrodynamic chromatography[17]. These systems have proven powerful and accurate, however, their operation takes relatively long periods of time, consumes large volumes of analytes, and often requires bulky, mechanically complex apparatus for regulating sample injection/fluid flows and for generating an external field or gradient in large fluidic channels or compartments.

Efforts to reduce volume and power requirements for particle separation have resulted in a number of miniaturized devices that take advantage of microfluidics and microfabrication. Owing to their small sizes, the microfabricated systems generally consume much smaller sample volumes and allow for faster separation. Furthermore, they enable more selective separation by facilitating precise manipulation of particles, and can attain higher separation efficiency by increasing effective field strength. Examples of such microfluidic devices include miniaturized centrifuge[18], micro-thermal FFF[19], micro-electrical FFF[20,21], micro-dielectrophoretic FFF[22], and other microfabricated particle sorters based on dielectrophoresis[23,24], magnetophoresis[25], acoustic waves[26], or optical interference patterns[27]. These methods, however, are still burdened by the need for external power sources generating driving forces for sample separation. In addition, on-chip integration of interfacing components such as mechanical moving parts, electrodes, heaters, optical lattice, or piezoelectric materials often complicates fabrication procedures and increases the complexity of resulting devices.

Alternative approaches to using microfabricated systems for particle separation can be found in microfluidic devices where size-dependent separation is achieved by filtering of particles through sieving structures[28-30] or by differential interaction of particles with local flow profiles[31-38]. By replacing the need for externally-applied forces with the use of microfabricated filters or laminar flows directed by carefully-designed channel geometries, these techniques permit simple, rapid, and power-efficient particle separation. Fabrication of microfluidic filtering components, however, is often not trivial if separation is based on sieving mechanism. Hydrodynamic particle separation depending on geometrically-driven laminar flows also requires external pumps for controlling flow rates and the position of particles in microchannels.

In this paper, we introduce a unique combination of field-driven separation with microhydrodynamics-assisted separation to accomplish rapid size-profiling, continuous mass-dependent separation, and isolation of particles in simple, self-contained microfabricated devices without using external pumps or power sources. In this method, we use the earth's gravity to drive fluid flows through microchannels as well as to induce differential sedimentation of particles according to their mass. Positional difference between particles initiated by sedimentation is further amplified hydrodynamically by laminar flows with widening flow streamlines, facilitating direct monitoring and isolation of fractionated subpopulations within short distances. This system also integrates particle separation with sample injection based on hydrodynamic focusing to increase separation resolution. We investigated hydrodynamic separation amplification both theoretically and experimentally. The capabilities of our system to perform simple, rapid, and high-purity continuous particle separation were demonstrated by sorting of polystyrene microbeads and purification of perfluorocarbon liquid droplets that are used in ultrasound imaging, magnetic resonance imaging, or embolotherapy[39-42].

Mechanism

The microfluidic sorting device with hydrodynamic separation amplification (μ-SOHSA) consists of three inlets, two inter-connected microchannels for sample focusing and separation, and collectors (Figure 1). In the sample focusing channel where fluid flows are driven parallel to gravity, polydisperse sample mixtures containing larger and smaller particles are introduced into the device through the middle inlet and hydrodynamically focused to the center of the focusing channel by flows of carrier liquid injected from the two side inlets (Figure 1A). After flowing around a 90° turn, the tightly focused stream of particles enters the separation channel whose upper wall is aligned perpendicular to gravity and lower wall gradually widens out. As the mean flow velocity becomes smaller due to the widening channel geometry, gravity takes effect and causes sedimentation of particles at a velocity given by $U_{sed} = 2r^2g\Delta\rho/(9\mu)$, where r is the radius of particles, g is gravitational acceleration, $\Delta\rho$ is the density difference between particles and carrier liquid, and μ is the viscosity of carrier liquid. For the particles with the same density, the equation suggests that the sedimentation velocity of larger particles is greater than that of smaller particles, resulting in difference in vertical position between larger and smaller particles. Concurrently, the asymmetrically-widening channel geometry generates flow profiles where the flow velocity in the direction of gravity is smaller near the horizontal upper wall and becomes larger in the areas closer to the widening lower wall, which gives rise to the widening of flow streamlines as the flow proceeds downstream. Therefore, larger particles that approach the lower channel wall more rapidly due to larger sedimentation velocities experience even greater downward motion than smaller particles do as they move downstream and as a result, the positional difference initially generated by sedimentation becomes even larger (Figure 1B and C. This hydrodynamic amplification of separation enables μ-SOHSA to perform particle separation more efficiently than is possible by the simple use of difference in sedimentation velocity. Mass-dependent particle sorting in μ-SOHSA is completed at the end of the separation channel where smaller and larger particles flow into the upper and lower collectors, respectively (Figure 1D).

Theory

We performed a theoretical analysis of hydrodynamic separation amplification by investigating the effect of the widening channel geometry on the trajectories of different-sized particles with the same density. Figure 2A shows a schematic diagram of the separation channel whose lower wall widens in the positive x-direction at an angle of θ Gravity is in the positive y-direction, and the width of the channel at the entrance and at any arbitrary longitudinal position along the x-axis are denoted by H_{in} and $H(x)$, respectively. To simplify the analysis, we considered the fluid flows in the microchannel to be two-dimensional in the xy-plane and ignored the flow domain and the movement of particles in the z-direction. Also, we assumed that there is no hydrodynamic interaction between particles.

Considering $\theta \ll 1$ and small Reynolds number of our system, the governing equations for the steady flow in the channel are given by

$$0 = -\frac{\mathbf{dp}}{\mathbf{dx}} + \mu\frac{\partial^2\mathbf{u}}{\partial\mathbf{y}^2} \text{ (Stokes equation)} \quad (1)$$

$$\frac{\mathbf{du}}{\mathbf{dx}} + \frac{\mathbf{d}\upsilon}{\mathbf{dy}} = 0 \text{ (Continuity equation)} \quad (2)$$

, where p is fluid pressure, μ is the viscosity of fluid, and u and υ are x- and y-directional flow velocities, respectively. Solving (1) and (2) using no-slip and no-penetration boundary conditions at the channel walls located at $y = 0$ and $y = H(x)$, we obtain the following expressions for the velocity components.

$$\mathbf{u}(\mathbf{x},\mathbf{y})=\frac{6\mathbf{Q}'}{(\mathbf{H}_{in}+\mathbf{x}\tan\theta)^3}\left[(\mathbf{H}_{in}+\mathbf{x}\tan\theta)\mathbf{y}-\mathbf{y}^2\right] \quad (3)$$

$$\upsilon(\mathbf{x},\mathbf{y})=\frac{6\mathbf{Q}'\tan\theta}{(\mathbf{H}_{in}+\mathbf{x}\tan\theta)^4}\left[(\mathbf{H}_{in}+\mathbf{x}\tan\theta)\mathbf{y}^2-\mathbf{y}^3\right] \quad (4)$$

, where Q' is a volumetric flow rate per unit thickness of the channel and H_{in} represents the entrance width of the separation channel. Assuming that a particle undergoing sedimentation follows the flow without causing any disturbance in the flow field, the distribution of the velocity at which the particle moves can be derived from (3) and (4) as $\underline{\boldsymbol{u}}_p = (\boldsymbol{u}_p, \boldsymbol{v}_p) = (\boldsymbol{u}(\boldsymbol{x}, \boldsymbol{y}), \boldsymbol{v}(\boldsymbol{x}, \boldsymbol{y}) + \boldsymbol{U}_{sed})$ Therefore, the equations dictating the Lagrangian motion of a particle are written as

$$\frac{\mathbf{dX}}{\mathbf{dt}}=\frac{6\mathbf{Q}'}{(\mathbf{H}_{in}+\mathbf{X}\tan\theta)^3}\left[(\mathbf{H}_{in}+\mathbf{X}\tan\theta)\mathbf{Y}-\mathbf{Y}^2\right] \quad (5)$$

$$\frac{\mathbf{dY}}{\mathbf{dt}}=\frac{6\mathbf{Q}'\tan\theta}{(\mathbf{H}_{in}+\mathbf{X}\tan\theta)^4}\left[(\mathbf{H}_{in}+\mathbf{X}\tan\theta)\mathbf{Y}^2-\mathbf{Y}^3\right]+\frac{2\mathbf{r}^2\mathbf{g}\Delta\rho}{9\mu} \quad (6)$$

Using (3) and (4), we first plotted streamlines in the separation channel for conditions matching the actual experimental configurations and the dimensions of μ-SOHSA. As shown in Figure 2B, separation between individual streamlines becomes larger progressively as the channel becomes wider in the downstream. Due to the asymmetric channel geometry, streamlines in the upper and middle regions maintain their orientation relatively parallel to the horizontal upper wall, whereas the widening channel wall prompts streamlines in the lower areas to deflect to a greater extent in the direction of gravity.

To demonstrate hydrodynamic amplification of particle separation, we generated three sets of trajectories traversed by a pair of polystyrene particles that are 1 and 20 μm in diameter in three different channel geometries, using equations (5) and (6). In a uniformly-narrow microchannel having parallel upper and lower walls separated by 500 μm, hydrodynamic transport of 1 and 20 μm particles resulted in a separation distance (δ_{p1}) of approximately 200 μm over the channel length of 2.5 cm (shown with dashed lines) (Figure 2C). Under the same flow conditions, however, the use of the widening channel with the same length led to more than five-fold increase in particle separation, and the distance between particles at the end of the channel (δ_w) was ~ 1.1 mm (shown with continuous lines) (Figure 2D). In a channel with a uniform width of 2.7 mm, 1 and 20 μm particles were separated by ~ 520 μm (δ_{p2}) (dashed-and-dotted lines in Figure 2C), which is less than 50 % of the separation in μ-SOHSA. These results demonstrate that the widening channel geometry of μ-SOHSA greatly assists in achieving more efficient mass-dependent sample separation by hydrodynamically amplifying sedimentation-driven separation between particles. Although it is possible to use uniformly-narrow microchannels having carefully-positioned splitters that can sort and isolate fractionated subpopulations even if separation is not pronounced (as in SPLITT), such tasks may demand very accurate monitoring of flow conditions to precisely direct sample streams to appropriate collectors and can be challenging when handling concentrated particle samples.

Experimental Section

Materials and Reagents

Poly(dimethylsiloxane) (PDMS) was obtained from Dow Corning Corp. (Midland, MI) and SU8 negative photoresist was purchased from MicroChem. Corp. (Newton, MA). Phosphate buffered saline (PBS) was obtained from Invitrogen Corp. (Carlsbad, CA), and bovine serum albumin (BSA) fraction V and fluorescein sodium salt from Sigma-Aldrich (St. Louis, MO).

Colored polystyrene microbeads with diameters of 3, 5, and 20 μm were purchased from Polysciences Inc. (Warrington, PA). perfluorocarbon (PFC) droplet emulsions were prepared by mixing saline, bovine serum albumin, and perfluorocarbon in a high-speed vial shaker (Crescent Dental Mfg. Co., Elgin, IL)[40]. For fluorescence imaging, PFC droplets were labeled with fluorescein isothiocyanate (FITC)[40].

Fabrication of μ-SOHSA and Flow Setup

Microchannels of μ-SOHSA with a thickness of 100 μm were created by casting PDMS prepolymer against a photolithographically-prepared SU8 mold and then sealed irreversibly onto a flat slab of PDMS using plasma oxidation. Before use, the entire device was treated with oxygen plasma for ~ 20 minutes to render the interior surfaces of the microchannel more hydrophilic, and briefly incubated with a BSA solution (10 mg/ml in DI water) to prevent adhesion of particles to channel surfaces. The channel was attached to an XY vertical stage (Newport, Irvine, CA) and oriented in the direction of gravity. Plastic reservoirs that can contain up to 3 ml of liquid were glued to the device and connected to the inlets via Tygon tubing (Fisher Scientific Inc., Hampton, NH). To isolate separated particle samples, upper and lower collector outlets were connected to Tygon tubing leading to plastic vials secured on a height-adjustable stage. Continuous, steady fluid flows were driven by height difference between the inlet and outlet reservoirs.

Visualization of Flow Streamlines

Fluorescein dissolved in a BSA solution (10 mg/ml in DI water) was used to indirectly visualize flow streamlines in a widening microchannel. Fluorescein solution was introduced into the middle inlet and hydrodynamically focused by incoming streams of non-fluorescent DI water from the side inlets. The flow rate of the sheath flows was varied to change the width of the middle fluorescent stream, and the resulting flows in the widening channel at different flow rates were captured by a CCD camera (Hamamatsu ORCA-ER) mounted on an epi-fluorescence microscope (Nikon TE-200).

Sizing and Sorting of Particles and PFC Droplets

Sample mixtures containing equal volumes of suspensions of polystyrene beads with different diameters or PFC droplet emulsions were introduced into the inlet reservoir, and the motion of particles/droplets was imaged by a digital camera (Nikon CoolPix 900) attached to a stereoscope (Nikon SMZ-1500). At the completion of separation, the samples collected at the outlet reservoirs were diluted with Isoton and further analyzed for enumeration and size-distribution measurements using a Coulter counter (Multisizer 3 Coulter counter, Beckman Coulter Inc.).

Results and Discussion

Flow Patterns

A key to hydrodynamic separation amplification in μ-SOHSA is a flow pattern where fluid streams spread progressively in response to the widening of the separation channel. We visualized this flow pattern in a widening microchannel, which is shown in Figure 3A. The pseudo-colored micrograph shows an overlay of fluorescence images taken at three different flow rates of the focusing streams from the side inlets that generated three different widths of the middle stream at the entrance of the widening channel. This image clearly illustrates that the sample streams widen gradually in the flow direction and their width nearly tripled at the end of the observation area spanning approximately 500 μm of channel length. Also, the boundary lines created by difference in fluorescence intensity between three streams visualize flow streamlines, and their spatial distribution reveals that the distance between individual

streamlines increases as the flow moves downstream. This is in contrast to flow patterns in a microchannel with a uniform width where unidirectional fluid motion maintains spacing between flow streamlines constant throughout the channel (Figure 3B).

Hydrodynamic Amplification of Particle Separation

To investigate the effect of widening flow streamlines on the efficiency of particle separation, we tested the separation of 1 and 20 μm particles in three different channel geometries: i) a uniformly narrow channel (width = 500 μm, length = 2.5 cm), ii) a uniformly wide channel (width = 2.7 mm, length = 2.5 cm), and iii) a typical separation channel of μ-SOHSA whose width increases from 500 μm to 2.7 mm over the length of 2.5 cm. Separation between particles was monitored at two prescribed locations along the length of microchannels, each of which represents the upstream and the downstream. Flow rates were maintained the same across the experiments (~ 1 ml/hr), and separation efficiency was evaluated qualitatively by comparing the distributions of two subpopulations in the downstream of the three different channels.

In a narrow microchannel, the sample stream remained tightly focused along the center and there was no discernible separation of particles in the upstream, mainly because of fast flow speed. Although a broadening of the particle stream was observed towards the downstream, 1 and 20 μm particles continued to stay in the vicinity of the center without any significant cross-stream migration towards the lower wall (Figure 3C). When a uniformly wide channel was used, the flow decelerated considerably upon entering the separation channel due to sudden increase in the channel width, permitting better tracking of the motion of particles. In the upstream, 20 μm particles were initially confined to the flow lamina in the center and gradually moved downward via sedimentation as the flow approached the outlet, separating them from 1 μm particles (Figure 3D). However, an overlap between the two populations still persisted. In the widening channel of μ-SOHSA, as shown in Figure 3E, the sedimentation-driven deviation of 20 μm particles from the initial streamlines along the center of the channel was observed to be substantially greater, and this resulted in a wide separation of the two components without any overlap in the downstream area within less than 30 seconds. By comparison, these results illustrate that the increasing width of the separation channel in μ-SOHSA enhances the resolution and efficiency of separation by gradually decreasing flow velocity and by creating spreading flow patterns so that the sedimentation in the vertical direction can be used in synergistic combination with the widening streamlines of flows in the horizontal direction to amplify separation between different-sized particles.

It should be noted that there is a lower limit of flow rate over which initial hydrodynamic focusing of particles in the vertical channel can be achieved, which is crucial for attaining high separation resolution by preventing the unwanted broadening of sample streams before they enter the separation channel. Also, the flow rate should be kept lower than a certain value over which flow becomes too fast and prevents sedimentation of particles. In the operational range of flow rate between these critical values, we found that separation performance of μ-SOHSA is always superior to that of the other two devices having the channels of uniform widths.

Particle Sorting and Size-Measurements

Figure 4A shows binary sorting of 1 and 20 μm polystyrene beads that are directed to flow into upper and lower collectors, respectively. The upper outlet channel leading to the upper collector was designed to be wider than the lower outlet channel to make the flow rate of the upper stream higher. According to the bifurcation law[43], particles traveling through a bifurcating region tend to flow into a daughter channel with a higher flow rate. Considering that the streams containing smaller particles usually lead to the bifurcating outlet junction of the separation channel, the imbalance of flow rate created by different channel widths facilitates guidance of smaller particles into the upper outlet channel. As shown in the micrograph, 1 μm particles

swerve into the upper outlet as they approach the bifurcation, whereas 20 μm particles distributed in the lower regions continue their linear motion and exit the separation channel through the lower outlet channel. The size-distribution measurements revealed that the purity of separated samples in each collector was nearly 100 % (Figure 4B).

For the separation of 3 and 20 μm polystyrene beads, the total flow rate was adjusted to be slightly higher (~ 1.2 ml/hr) than that used in the separation of 1 and 20 μm particles (~ 1 ml/hr) to counteract the larger sedimentation velocity of 3 μm particles and to prevent them from streaming into the lower outlet. Figure 4C captures the particle separation at the outlet junction where a stream of 3 μm particles in red is drawn into the upper outlet and individual dots showing 20 μm particles are advancing to the lower outlet microchannel. As in the previous case, a post-separation analysis showed ~ 100 % purity of fractionated subpopulations with a negligible overlap between their size-distributions (Figure 4D).

Sorting of Perfluorocarbon (PFC) Liquid Droplets

Use of liquid droplets encapsulating PFC as contrast agents or tracers has gained increasing popularity in ultrasound or magnetic resonance imaging[1]. Furthermore, acoustic vaporization of superheated PFC liquid droplets into large gas bubbles that can be trapped in microvasculatures and block blood stream is considered to have great potential in embolotherapy for cancer treatment[39-41]. The most frequently used methods of producing PFC droplets include sonication or high-speed mechanical shaking of mixture solutions containing PFC, saline, and BSA[40]. These methods, however, often result in polydisperse emulsions containing larger droplets that are not transpulmonary and can potentially be harmful by causing undesired blockage of blood stream and tissue damage. Therefore, it is necessary to remove the larger PFC droplets that are larger than 6 μm in diameter[39,40]. As an alternative to conventional filtering methods based on syringe filter discs and high pressures, which can be mechanically invasive to deformable liquid droplets, we used μ- SOHSA to isolate transpulmonary droplets that are smaller than 6 μm.

Figure 5A shows a micrograph of polydisperse PFC droplet population before separation. The mean diameter was 4.486 μm, and approximately 25 % of the droplets had diameters larger than 6 μm. When the focused stream of the PFC droplets was introduced into the separation channel of μ-SOHSA, a majority of smaller droplets were distributed along the center appearing as a bright fluorescent band, and larger droplets were observed to migrate continuously towards the lower channel wall to different extents depending on their size (Figure 5B). The size measurements of the droplets isolated into the upper collector showed that ~ 99. 97 % of the collected sample is smaller than 6 μm and that the mean diameter of droplets was reduced to 2.147 μm (Figure 5C). Optical observation confirmed exclusive retrieval of smaller droplets and removal of larger ones as can be seen in Figure 5D. The population collected at the lower outlet was found to have a mean diameter of 6.824 μm (Figure 5E) and to consist mainly of larger droplets (Figure 5F). The yield of separation, which is defined as the ratio of the number of target PFC droplets (smaller than 6 μm in diameter) retrieved from the upper collector to the total number of target droplets injected into the middle inlet, was evaluated to be approximately 73 %.

It is worthwhile to note that the separation yield can be raised by positioning the stream carrying a majority of target droplets farther away from the lower channel wall to prevent the loss of smaller droplets to the lower outlet, which can be accomplished simply by increasing the flow rate in the separation channel. In doing so, however, we found that larger droplets can be easily entrained into the target sample stream and flow into the upper outlet, which lowers purity of separation and more importantly, allows potentially harmful larger droplets to be present in the target population.

Conclusion

Miniaturization of conventional separation systems based on the combination of gravity and hydrodynamic flows such as gravitational FFF[11], sedimentation FFF[44,45], and gravity SPLITT[12] has been challenging because the separation resolution in these systems is proportional to the residence time of sample particles, which often requires long fluidic channels. Hydrodynamic separation amplification presented in this work offers an alternative means to realize gravity-driven separation in microfabricated devices without sacrificing separation resolution, sample retrieval efficiency, or analysis time.

Use of the earth's gravity in μ-SOHSA greatly simplifies the operation and reduces volume/power requirements of the device significantly by eliminating the need for other external force or field for generating fluid flows and sedimentation of sample particles. Combined with optically transparent fluidic channels, orderly laminar flows without any random variations in μ-SOHSA confer the ability to monitor and manipulate fluid streams and the movement of particles in real time, making this system attractive for testing and optimizing separation and sorting of various types of particles. Also, separation in μ-SOHSA is gentle and does not impose any damaging mechanical stresses on sample particles, which can be beneficial for sustaining the viability of living analytes throughout separation or for handling delicate samples. The self-contained nature of μ-SOHSA with no need for external power supplies and its simple operation provide opportunities to develop small, portable, and disposable point-of-care medical diagnostic tools, which may be of particular interest for developing countries where the availability of diagnostic technologies is very limited[46,47].

Sample separation demonstrated in our work, however, is limited to the separation of particle populations with relatively large size-difference. For more widespread application, the use of hydrodynamic separation amplification for high-resolution separation needs to be further investigated. This may require the manipulation and optimization of flow conditions and widening channel geometry. Also, small velocities of fluid flows in our device can be disadvantageous for preparative sample separation and isolation, which may be resolved by designing arrays of separation microchannels operating in parallel to achieve higher throughputs.

We believe that μ-SOHSA will serve as a useful measurement and separation tool for a broad range of analytical and preparative applications.

Acknowledgement

We thank Xiaoyue Zhu, Brian Johnson, and Mark Burns for assisting in channel fabrication and for providing access to microfabrication facilities. This research was supported by the Whitaker Foundation, Horace H. Rackham Graduate Studies at the University of Michigan, NSF (BES 0238625), NIH (EB00281), and US Army Grant No. DAMD17-00-1-0344.

References

1. Caldwell KD, Cheng ZQ, Hradecky P, Giddings JC. Cell Biophys 1984;6:233–251. [PubMed: 6085558]
2. Caldwell KD, Karaiskakis G, Giddings JC. J. Chromatogr 1981;215:323–332.
3. Giddings JC, Yang FJ, Myers MN. Anal. Biochem 1977;81:395–407.
4. Blanda M, Reschiglian P, Dondi F, Beckett R. Polymer International 1994;33:61–69.
5. Moon MH, Giddings JC. Anal. Chem 1992;64:3029–3037.
6. Myers MN, Chen P, Giddings JC. ACS Symp. Ser 1993;521:47–62.
7. Levin S, Nudelman R, Reschiglian P, Pasti L. J. Pharm. Biom. Anal 1995;13:869–877.
8. Taylor HE, Garbarino JR, Murphy DM, Beckett R. Anal. Chem 1992;64:2036–2041.

9. McCarthy JF, Zachara JM. Environ. Sci. Technol 1989;23:496–502.
10. Albright KL, Cram LS, Martin JC. ACS Symp. Ser 1991;464:73–88.
11. Giddings JC. Science 1993;260:1456–1465. [PubMed: 8502990]
12. Fuh CB. Anal. Chem 2000;72:266A–271A.
13. Radko SP, Stastna M, Chrambach A. Anal. Chem 2000;72:5955–5960. [PubMed: 11140762]
14. Radko SP, Stastna M, Chrambach A. Electrophoresis 2000;21:3583–3592. [PubMed: 11271475]
15. Scott CD. Anal. Biochem 1968;24:292–298. [PubMed: 5671027]
16. Husain A, Hamielec AE, Vlachopoulos J. J. Liq. Chromatogr. R. T 1981;4:295–320.
17. Small HJ. J. Colloid. Interface Sci 1974;48:147–161.
18. Marziali A, Willis TD, Davis RW. Proc. Natl. Acad. Sci. USA 1999;96:61–66. [PubMed: 9874772]
19. Edwards T, Gale BK, Frazier AB. Anal. Chem 2002;74:1211–1216. [PubMed: 11922286]
20. Gale BK, Caldwell KD, Frazier AB. Anal. Chem 2002;74:1024–1030. [PubMed: 11924959]
21. Gale BK, Caldwell KD, Frazier AB. IEEE Trans. Biomed. Eng 1998;44:1459–1469. [PubMed: 9835194]
22. Markx GH, Rousselet J, Pethig R. J. Liq. Chromatogr. R. T 1997;20:2857–2872.
23. Kang KH, Kang YJ, Xuan XC, Li DQ. Electrophoresis 2006;27:694–702. [PubMed: 16385598]
24. Chen DF, Du H, Li WH. J. Micromech. Microeng 2006;16:1162–1169.
25. Pamme N, Manz A. Anal. Chem 2004;76:7250–7256. [PubMed: 15595866]
26. Petersson F, Nilsson A, Jonsson H, Laurell T. Anal. Chem 2005;77:1216–1221. [PubMed: 15732899]
27. MacDonald MP, Spalding GC, Dholakia K. Nature 2006;426:421–424. [PubMed: 14647376]
28. Sethu P, Sin A, Toner M. Lab Chip 2006;6:83–89. [PubMed: 16372073]
29. Zhu L, Zhang Q, Feng HH, Ang S, Chauc FS, Liu WT. Lab Chip 2004;4:337–341. [PubMed: 15269801]
30. Chen Z, Zhang S, Tang Z, Xiao P, Guo X, Lu Z. Surf. Interface Anal 2006;38:996–1003.
31. Yamada M, Nakashima M, Seki M. Anal. Chem 2004;76:5465–5471. [PubMed: 15362908]
32. Yamada M, Seki M. Anal. Chem 2006;78:1357–1362. [PubMed: 16478134]
33. Nam KH, Chang WJ, Hong H, Lim SM, Kim DI, Koo YM. Biomed. Microdevices 2005;7:189–195. [PubMed: 16133806]
34. Yamada M, Kasim V, Nakashima M, Edahiro J, Seki M. Biotechnol. Bioeng 2004;88:489–494. [PubMed: 15459911]
35. Yamada M, Seki M. Lab Chip 2005;5:1233–1239. [PubMed: 16234946]
36. Yang S, Undar A, Zahn JD. Lab Chip 2006;6:871–880. [PubMed: 16804591]
37. Zhang X, Cooper JM, Monaghan PB, Haswell SJ. Lab Chip 2006;6:561–566. [PubMed: 16572220]
38. Huang LR, Cox EC, Austin RH, Sturm JC. Science 2004;304:987–990. [PubMed: 15143275]
39. Kripfgans OD, Fowlkes JB, Woydt M, Eldevik OP, Carson PL. IEEE Trans. Ultrason. Ferroelectr. Freq. Control 2002;49:726–738. [PubMed: 12075966]
40. Kripfgans OD, Fowlkes JB, Miller DL, Eldevik OP, Carson PL. Ultrasound Med. Biol 2000;26:1177–1189. [PubMed: 11053753]
41. Kripfgans OD, Fowlkes JB, Woydt M, Eldevik OP, Carson PL. J. Acoust. Soc. Am 2004;116:272–281. [PubMed: 15295987]
42. Bull JL. Crit. Rev. Biomed. Engr 2005;33:299–346.
43. Fung YC. Microvasc. Res 1973;5:34–48. [PubMed: 4684755]
44. Giddings JC, Yang FJ, Myers MN. Anal. Chem 1974;46:1917–1924.
45. Giddings JC, Myers MN, Moon MH, Barman BN. ACS Symp. Ser 1991;472:198–216.
46. Yager P, Edwards T, Fu E, Helton K, Nelson K, Tam MR, Weigl BH. Nature 2006;442:412–418. [PubMed: 16871209]
47. Toner M, Irimia D. Annu. Rev. Biomed. Eng 2005;7:77–103. [PubMed: 16004567]

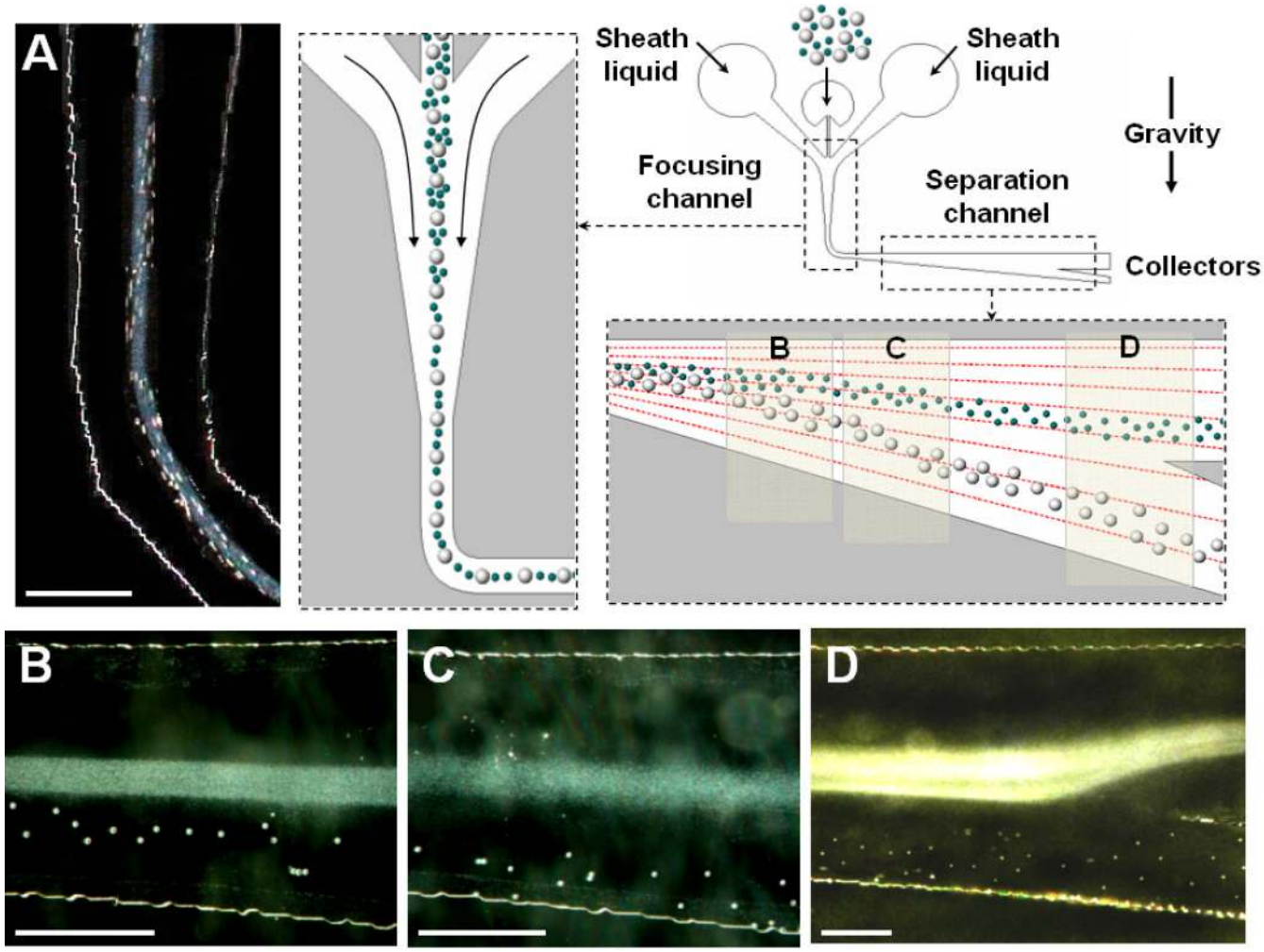

Figure 1.

Mass-dependent particle separation based on hydrodynamic amplification of sedimentationdriven particle separation in μ-SOHSA. (A) Particles are introduced into the middle inlet and hydrodynamically focused by sheath flows in the sample focusing channel. Upon entering the separation channel where the flow direction is aligned perpendicular to gravity, sedimentation of particles occurs, and resulting difference in the vertical position between larger (white polystyrene beads, 20 μm in diameter) and smaller (blue polystyrene beads, 1 μm in diameter) particles is gradually amplified by asymmetrically widening flow streamlines generated by widening channel geometry as shown in (B) and (C). (D) In the far downstream, isolation of separated particles is achieved by directing each particle stream to different outlet channels. Fluid flows in μ-SOHSA are driven by the earth's gravity. The separation demonstrated here was performed at a total flow rate of ~ 1 ml/hr. Size bar, 500 μm.

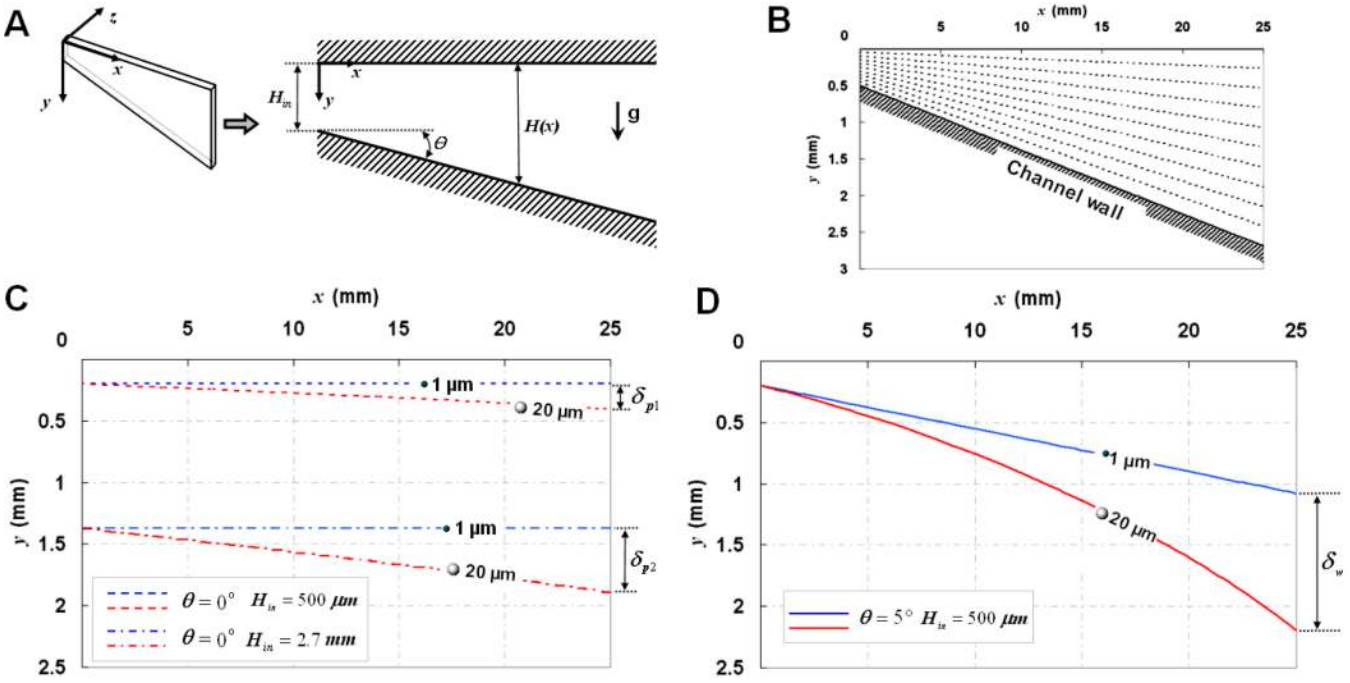

Figure 2.

Theoretical analysis of hydrodynamic separation amplification. (A) A two-dimensional model of a hydrodynamic flow in the separation channel of μ-SOHSA. (B) Widening flow streamlines in the separation channel at a typical flow rate used in μ-SOHSA. (C) Trajectories of 1 and 20 μm particles with the same density in a parallel-plate microchannel having a uniform width of (C) 500 μm (dashed lines) or 2.7 mm (dashed-and-dotted lines), compared to those in (D) the widening separation channel of μ-SOHSA that widens from 500 μm to 2.7 mm over the length of 2.5 cm (continuous lines). Q' was set at 2.8×10^{-5} m^2/sec, corresponding to 1 ml/hr in the actual device. It can be seen that terminal separation in μ-SOHSA (δ_w) is much greater than that in the uniformly narrow or wide microchahnel (δ_{p1} or δ_{p2}).

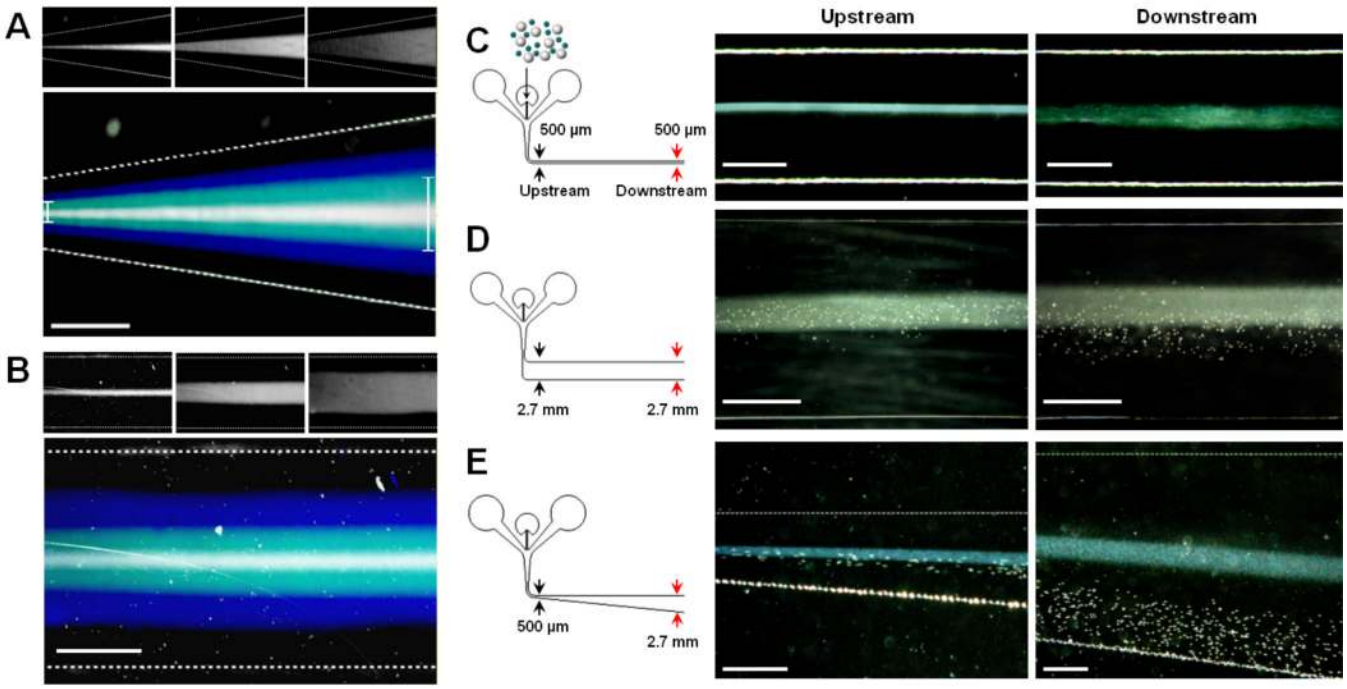

Figure 3.

Flow patterns in a widening microchannel and experimental demonstration of hydrodynamic separation amplification in μ-SOHSA. (A) Fluorescence imaging of fluorescein streams in a widening microchannel reveals spreading flow patterns and widening flow streamlines. (B) In a microchannel having a uniform width, the flow maintains its unidirectional motion and the distance between individual streamlines remains unchanged throughout the length of the channel. The top three images in each figure show three different fluorescent sample streams with different widths at the entrance of the channel. Size bar, 100 μm. Under the same flow conditions, separation of 1 and 20 μm polystyrene beads in μ-SOHSA shown in (E) is greater than that in a microchannel with a constant width of (C) 500 μm or (D) 2.7 mm. Size bars in (C), (D), and (E) show 250, 1000, and 500 μm, respectively.

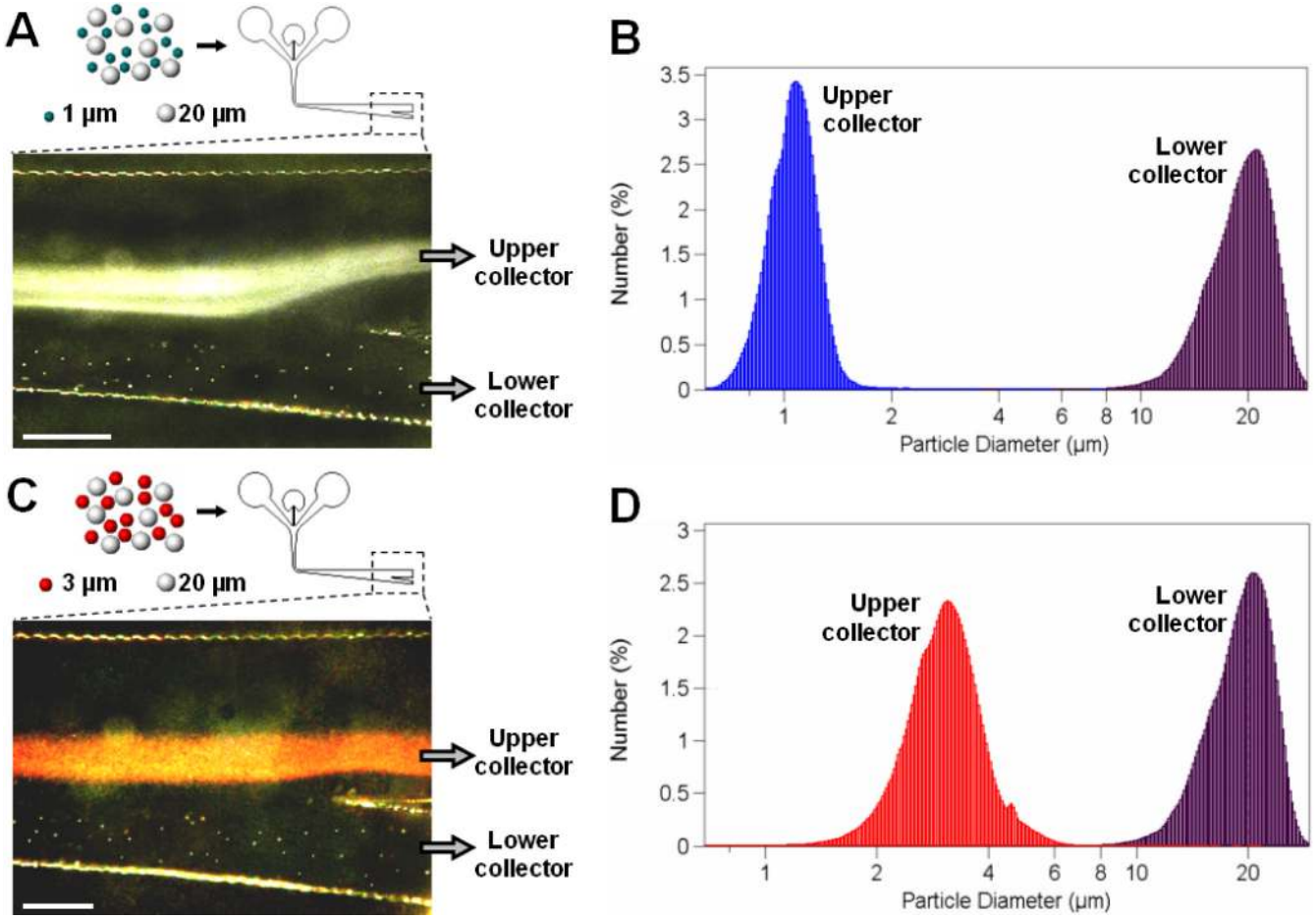

Figure 4.

Binary sorting of different-sized polystyrene beads in μ-SOHSA. As illustrated in (A) and (C), the bifurcating junction at the end of the separation channel enables sorting and isolation of separated subpopulations by prompting smaller (1 or 3 μm) and larger (20 μm) particles to flow into the upper and lower outlet microchannels, respectively. Size-distribution measurements shown in (B) and (D) demonstrate ~ 100 % purity of separated samples retrieved from each collector. Size bar, 500 μm.

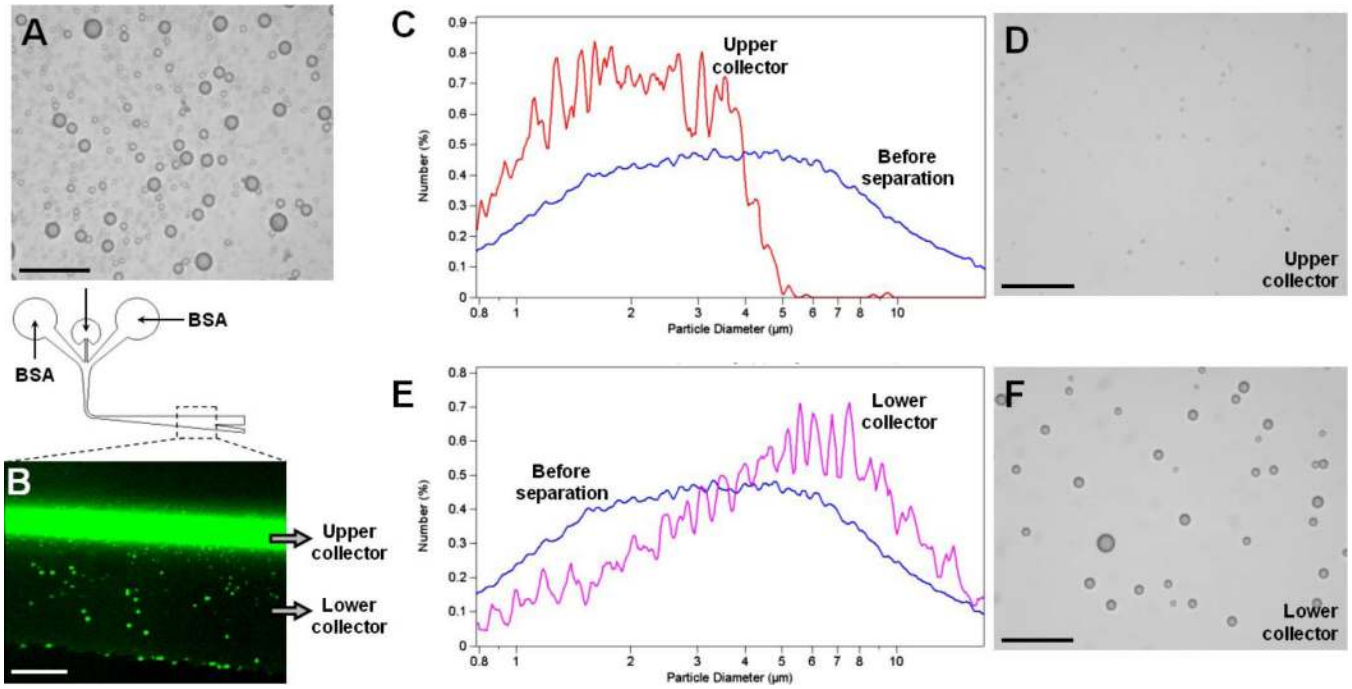

Figure 5.

Sorting and purification of PFC liquid droplet emulsions. (A) A polydisperse population of PFC droplets produced by high-speed shaking. Size bar, 150 μm. (B) Distribution of PFC droplets in the separation channel of μ-SOHSA. Larger droplets are separated from a fluorescent stream of smaller droplets and are positioned in the lower region. Size bar, 500 μm. (C) This separation successfully isolates target droplets (< 6 μm) into the upper collector, which can be optically confirmed by the micrograph of smaller droplets shown in (D). (E) & (F) Larger droplets are driven selectively into the lower collector and removed from the original population. Size bar, 150 μm.